Dual-Output Extended-Power-Range Quasi-Resonant Inverter for Induction Heating Appliances

Héctor Sarnago, *Senior Member, IEEE*, Óscar Lucía, *Senior Member, IEEE*, and José M. Burdío, *Senior Member, IEEE*.
Department of Electronic Engineering and Communications, I3A
Universidad de Zaragoza
Zaragoza, Spain
hsarnago@unizar.es, olucia@unizar.es

[1]*Abstract*— **Induction heating technology provides efficient and reliable heating processes that outperforms other classical heating methods based on fossil fuels or resistive heating. Among its many industrial, domestic and biomedical applications, domestic induction heating appliances are a popular choice due to these advantages. This technology requires high-performance and cost-effective inverters that takes the most of the power devices and the converter topology. Depending upon the desired performance and output power range, different power converters are employed. However, currently, most platforms rely on the well-known series resonant half-bridge topology. Single-switch topologies offer a cost-effective implementation but are limited to the low-cost low-performance markets due to their limitations in terms of output power and power control.**

In this context, this paper proposes a high-performance dual-output quasi-resonant inverter for modern induction heating appliances. Unlike state-of-the-art proposals, this converter achieves full output power operating range up to 3.6 kW. Consequently, it provides a high-performance cost-effective alternative to current implementations. The proposed converter is analyzed in this paper and experimentally verified using a dual-output 3.6-kW induction heating appliance prototype.

Keywords—Induction heating, home appliance, inverter, class-E, efficiency, resonant power conversion.

I. INTRODUCTION

Induction heating (IH, Fig. 1) has become a leading application of wireless power transfer to the domestic area in the medium power range [1, 2]. This technology exhibits clear benefits in terms of performance, safety, and efficiency [3], and it provides superior user performance, making it a very interesting alternative in the current market. Advances in power electronics, magnetic component design and digital control have made possible to replace classical heating techniques such as gas or electric resistive stoves.

IH technology requires efficient and cost-effective inverters in order to operate in a wide output power range. The operation output range varies typically from 500 W up to 3.6 kW. In the past, different resonant converter topologies [4] have been proposed depending on the required output power and final applications. Firstly, single-switch quasi-resonant inverters, usually based on the class-E-like converters [5-7] or other quasi-resonant implementations [8], have been widely used for low-power induction systems that feature constant induction heating load. These converters
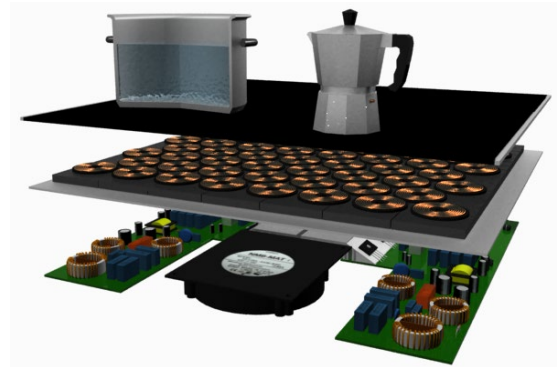

Fig. 1. Flexible induction heating appliance: multi-coil systems improve user performance.

provide a simplified implementation of the classical class-E converter, enabling soft-switching operation while maintaining a cost-effective implementation. These implementations can be achieved using ZVS or ZCS configurations [9] (Fig. 2). However, ZVS is often preferred because it does not require an additional coil. While the main advantage of this topology is its simplicity and low cost, the limited output power, typically up to 2 kW or lower [10-16] due to the voltage in the power device, and limited control capabilities limits its adoption. This is mainly due to the maximum allowed voltage in the power devices. This technology has wide adoption in markets where water-boiling processes are predominant or cost-oriented markets. On the other hand, full [17-22] and half-bridge [23-28] resonant inverters, also called class-D converters, have been proposed for high-medium output power levels. Those topologies feature higher output power capabilities and improved power control with increased complexity and cost. Currently, the half-bridge series resonant inverter is the most used topology because its good performance-cost balance up to the 3.6 kW output power range. Other approaches include multi-inductor [29-33], high-efficiency [34], or selectable induction heating target systems [35, 36]. Besides, several direct ac-ac converters have been proposed for IH applications [37-40], reducing the number of components and increasing the efficiency and performance. However, current design trends are moving towards cost-effective implementations that can achieve the high performance demanded by the user, forcing the designer to develop new optimized power converter topologies.

In this context, this paper proposes a reconfigurable dual-output quasi-resonant inverter focused on providing an efficient and cost-effective operation in the whole required operating range. The main benefit of the proposed converter is that it achieves full output power range up to 3.6 kW, i.e.

the whole operating range of state-of-the-art half-bridge-based appliances, with improved output power control and a cost-effective implementation. This is done by means of a reconfigurable resonant capacitor. This will enable the development of high-end domestic induction heating appliances with a cost-effective implementation. The main advantage of this proposal is therefore to be able to provide a full-output-power range implementation using a single-switch topology thanks to the use of an adaptable resonant network. Consequently, a high-performance cost-effective implementation is achieved.

The remainder of this paper is organized as follows. Section II details the proposed power converter, focusing on the proposed topology, operation modes, operating regions, and soft-switching control strategy. Besides, the main equations describing the circuit operation and the converter design criteria, taking into account the power devices and

operating points, are given. Section III details the main implementation and experimental results. A real scale dual-output domestic IH prototype featuring the proposed topology has been built using the proposed topology. The main experimental waveforms are presented and discussed, proving the feasibility of the proposed topology. Finally, Section IV summarizes the conclusions of this paper.

II. PROPOSED POWER CONVERTER

A. Proposed single-switch dual-output quasi-resonant inverter

The proposed power converter is based on the single-switch quasi-resonant inverter topology [6, 41]. This converter can be implemented following different structures, as it is shown in Fig. 3. These alternatives exhibit different current ratios between the rms and average bus current, and alternatives (b) and (c) mitigates the effect of the power device output capacitance. Considering the minimum current ratio between these alternatives to minimize current and, therefore, maximize efficiency, and the use of IGBT technology with negligible output capacitance, the high-side resonant capacitor is selected as base topology. Consequently, the proposed topology is based on a single-switch quasi-resonant inverter that enables reconfiguration of the resonant tank (Fig. 4) using R_1 and R_2 switches. The resonant capacitors C_r and power devices M_i can be reconfigured to supply two IH loads in optimized operating conditions, reducing the blocking voltage at maximum output power. Each IH load is modelled by its equivalent resistance and inductance, R_{eq}-L_{eq} [42-44]. Besides, this topology can be extended to supply a higher number of loads if required.

The main benefit of the proposed topology is that the reconfigurable resonant tank allows to adapt the voltage in the power device to maximize the maximum achievable output power. As a consequence of this, it allows to optimize
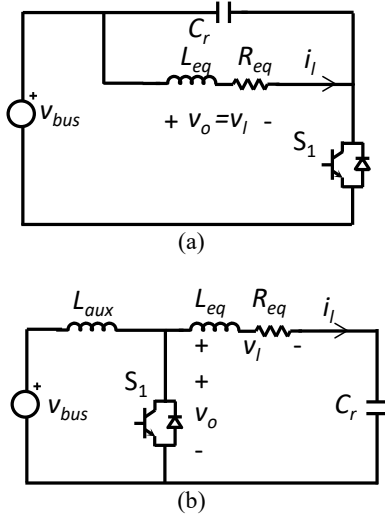

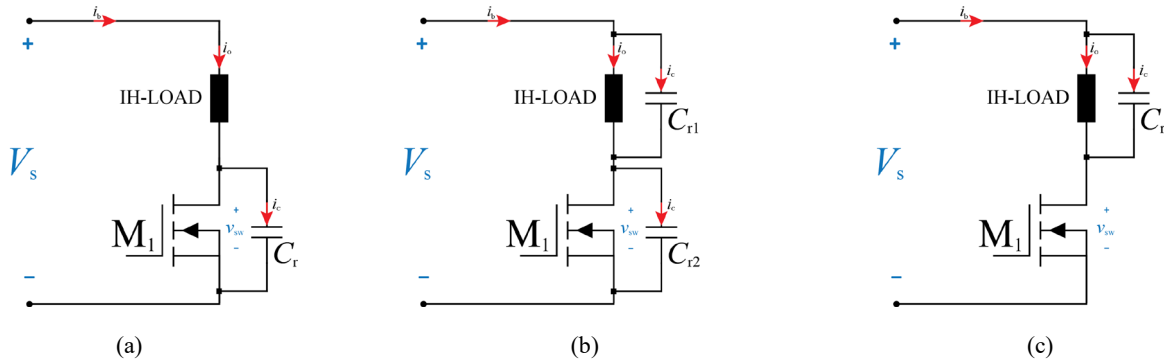Fig. 2. Single-switch implementations for induction heating applications: (a) ZVS and (b) ZCS.

Fig. 3. Single-switch quasi-resonant inverter alternative configurations: (a) high-side resonant capacitor, (b) low-side resonant capacitor and (c) split resonant capacitor.
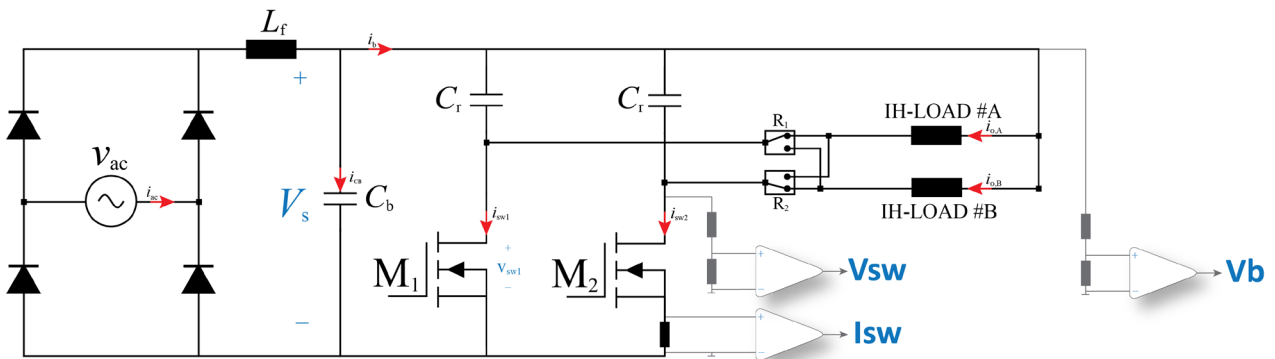

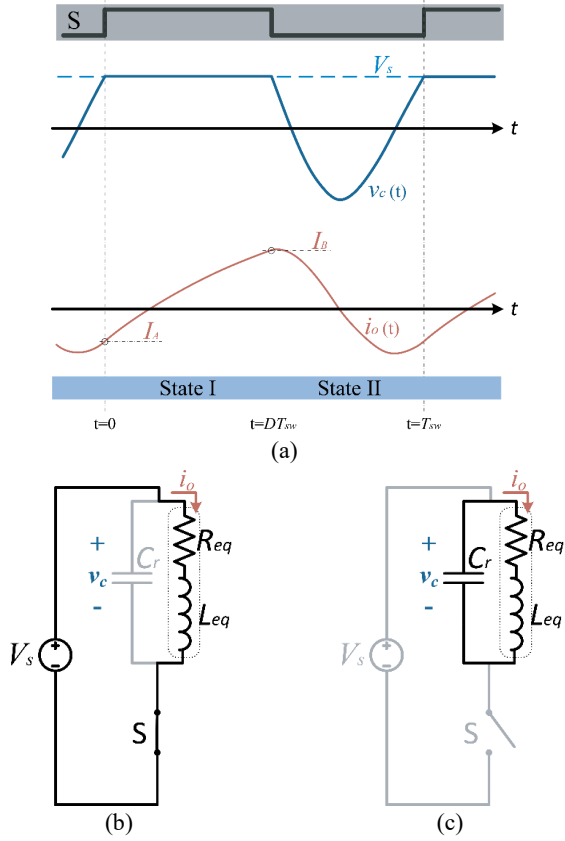Fig. 4. Proposed quasi-resonant dual inverter.

Fig. 5. Proposed single-switch quasi-resonant converter main waveforms (a) and equivalent circuits (b-c).

the quasi-resonant topology operation, enabling to reach the complete output power range, i.e. up to 3600 W per load, without exceeding the power devices maximum voltage ratings. This enables to use this topology, not only for low-end cost-effective appliances, but also of high-end implementations. Besides, the proposed topology can be easily extended to power total-active-surface appliances by replicating the proposed structure.

Fig. 5 summarizes the main converter waveforms and equivalent operational states. The proposed converter follows a single-switch quasi-resonant operation, achieving zero voltage switching (ZVS) and, consequently, ensuring soft-switching and high efficiency. In these topologies, ensuring soft-switching is a challenging tasks, because the operating point, i.e. voltage and current in the device, highly depends on the operating conditions and the IH load. However, the proposed topology and control strategy achieves full soft-switching operation as it is shown in the experimental results section.

During the switching cycle, the converter has two different states as in (Fig. 5(b,c)). When the switching device are activated (State I), the equivalent circuit is a series RL. This configuration is considered non-resonant because the resonant capacitor is short-circuited to the supply voltage source, and thus

$$v_c(t) = V_s, \quad (0 \le t \le DT_{sw}). \tag{1}$$

The load current, i_o, results

$$i_o(t) = \frac{V_s}{R_{eq}} - \left(\frac{V_s}{R_{eq}} - I_A\right)e^{-\frac{R_{eq}}{L_{eq}}t}, \quad (0 \le t \le DT_{sw}). \tag{2}$$

Where I_A, is the initial load current value, and I_B

represents the final load current at $t=DT_{sw}$ for state I, D is the duty cycle, and DT_{sw} is the time length of State I.

When the switching device is turned off, State II, the equivalent circuit is an RLC circuit composed of the electrical equivalent of the induction heating load and the resonant capacitor. This configuration is resonant and provides the required current oscillation to achieve ZVS. Equation (3) expresses the set of solutions [45] of the differential equation that describes the resonant capacitor voltage

$$v_c(t) = e^{-\xi(t-DT_{sw})}\begin{pmatrix} k_1\sin(\omega_n(t-DT_{sw})) + \\ k_2\cos(\omega_n(t-DT_{sw})) \end{pmatrix}, \left(DT_{sw} < t \le T_{sw}\right) \tag{3}$$

where $\xi = R_{eq}/2L_{eq}$ is the damping factor and $\omega_o = 1/\sqrt{L_{eq}C_r}$, $\omega_n = \sqrt{\omega_o^2 - \xi^2}$ are the resonant and natural angular frequencies, respectively. Thus, the load current, i_o, in State II results

$$i_o(t) = -C_r\frac{dv_c(t)}{dt} =$$
$$= C_r e^{-\xi(t-DT_{sw})}\begin{pmatrix} \sin(\omega_n(t-DT_{sw}))[V_s\omega_n + \xi k_1] + \\ \cos(\omega_n(t-DT_{sw}))[V_s\xi - k_1\omega_n] \end{pmatrix}, \quad (DT_{sw} < t \le T_{sw}). \tag{4}$$

Assuming a soft-switching ZVS operation, four boundary conditions are established for the steady-state operation, as it can be seen in Fig. 5:

$$\begin{cases} I_A = i_o(t = T_{sw}) \\ I_B = i_o(t = DT_{sw}) \\ V_s = v_C(t = T_{sw}) \\ V_s = v_C(t = DT_{sw}) \end{cases}. \tag{5}$$

By solving the inductor current restrictions two design conditions are obtained:

$$I_A = C_r e^{-\xi T_{sw}(1-D)}\begin{pmatrix} \sin(\omega_n T_{sw}(1-D))[k_2\omega_n + \xi k_1] + \\ \cos(\omega_n T_{sw}(1-D))[k_2\xi - k_1\omega_n] \end{pmatrix}, \tag{6}$$

and replacing I_B from (2) at $t=DT_{sw}$, the second boundary condition results

$$\frac{V_s}{R_{eq}} - \left(\frac{V_s}{R_{eq}} - I_A\right)e^{-\frac{R_{eq}}{L_{eq}}DT_{sw}} = C_r\left(k_2\xi - k_1\omega_n\right). \tag{7}$$

Besides, by applying the resonant capacitor voltage restrictions (third and fourth boundary conditions), k_1 and k_2 result

$$k_1 = \frac{\left(e^{\xi(1-D)T_{sw}} - \cos(\omega_n(1-D)T_{sw})\right)}{\sin(\omega_n(1-D)T_{sw})}V_s, \tag{8}$$

$$k_2 = V_s. \tag{9}$$

Thus, the converter temporal waveforms are defined, and as a result, key converter parameters can be obtained. On the other hand, input power can be calculated by means of the average input current, I_s,

$$I_s = \frac{1}{T_{SW}}\int_0^{T_{SW}} i_s(t)dt = \frac{1}{T_{SW}}\int_0^{DT_{SW}} i_o(t)dt, \tag{10}$$
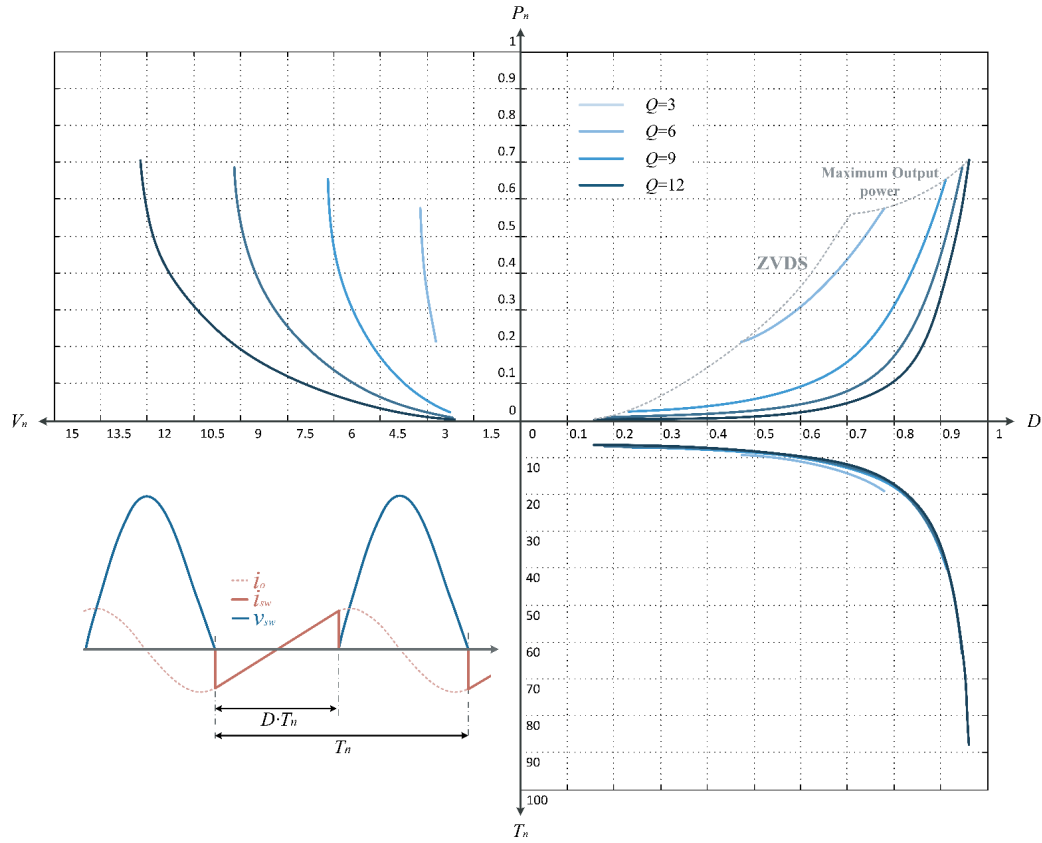
thus, the average input power, P, is

Fig. 6. Single-switch quasi-resonant inverter operating regions for different operating conditions and induction heating loads characterized by their quality factors, Q: output power versus power device blocking voltage (top left) and duty cycle (top right), where soft-switching limits are highlighted; switching period versus duty cycle (bottom right); and main waveforms (bottom left).

$$P = V_s I_s = \frac{V_s^2}{R_{eq} T_{sw}} \int_0^{DT_{sw}} \left[1 - \left(1 - \frac{I_A R_{eq}}{V_s} \right) e^{-2\xi t} \right] dt, \quad (11)$$

resulting

$$P = \frac{V_s^2}{R_{eq} T_{sw}} \left[DT_{sw} + \frac{1}{2\xi} \left(1 - \frac{I_A R_{eq}}{V_s} \right) \left(e^{-2\xi DT_{sw}} - 1 \right) \right]. \quad (12)$$

As a result, Fig. 6 shows the normalized design plane for the proposed converter. This diagram includes the output power versus the power device blocking voltage (top left) and duty cycle (top right) for different operating points and induction heating loads defined by their quality factors, Q. Besides, the switching period versus duty cycle is shown (bottom right), together with the main waveforms (bottom left). A set of normalized parameters have been used to extend analytical results. Where $T_n = \omega_n T_{sw}$, is the normalized switching period, $P_n = P / \left(V_s^2 / R_{eq} \right)$, represents the normalized input power, and $V_n = \hat{V}_{swtich} / V_s$, is the normalized switch peak voltage. The normalized output power as a function of control parameters (D, T_n) for different load quality factors, $Q = \omega_o L_{eq} / R_{eq}$, have been obtained. This diagram can be used to select the operating conditions to obtain a desired maximum output power with a maximum blocking voltage that is limited by the power device used. This analysis and operating curves can be extended to the case of the maximum power range, by changing the capacitor value accordingly, or to the
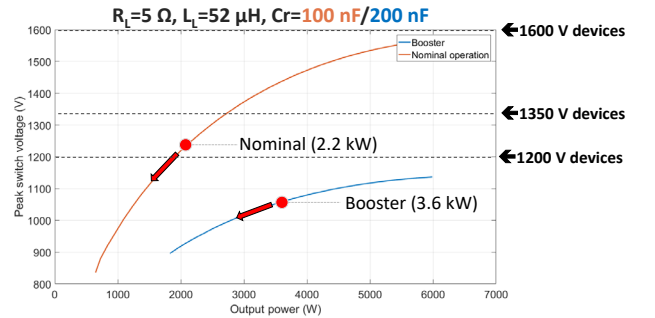

Fig. 7. Design example for different power device ratings and output power: single resonant capacitor (red line) and paralleled resonant capacitor (blue line).

independent parallel operation of the two inverters.

As it can be seen in this figure, the power device maximum voltage, V_n, limits the maximum achievable output power, being critical in real domestic IH applications. The proposed topology takes advantage of the configurable resonant tank to take the most of the power converter. Consequently, by modifying the resonant capacitor the operating point is moved, so the maximum output power can be reached without exceeding the power device maximum ratings.

Fig. 7 shows the available operating curves when operating with a single capacitor (red line) or with paralleled capacitors (blue line). This figure highlights the main benefit of the proposed topology, that enables to maximize the operating range by limiting the maximum voltage. The

(a)   (b)
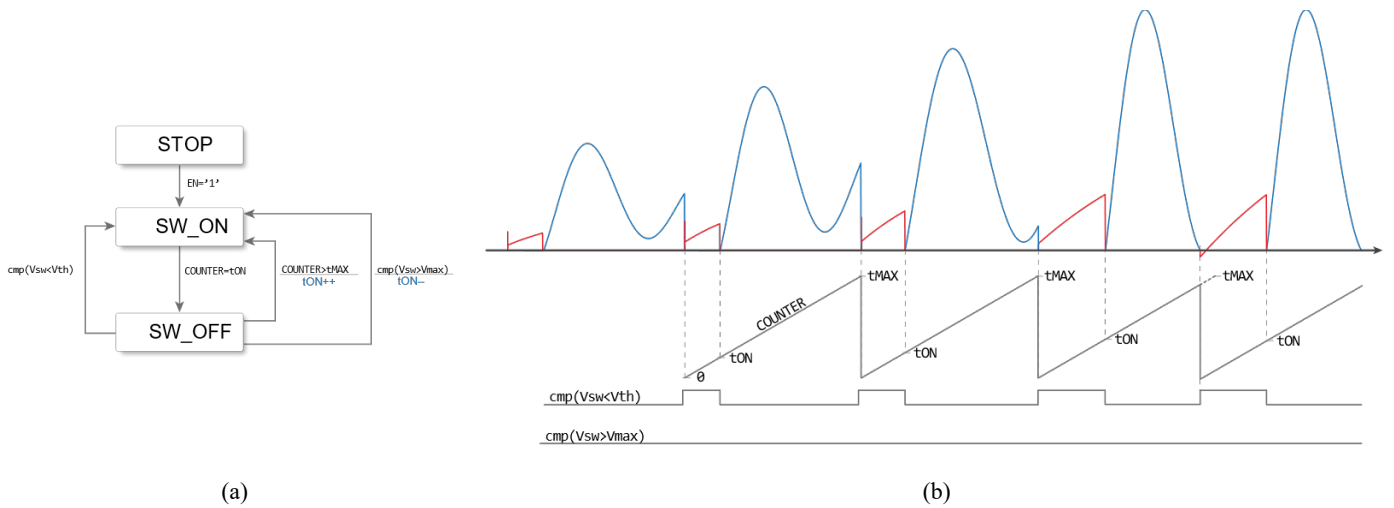
Fig. 8.   Proposed control strategy to ensure soft-switching: (a) control algorithm and (b) main waveforms and digital signals.
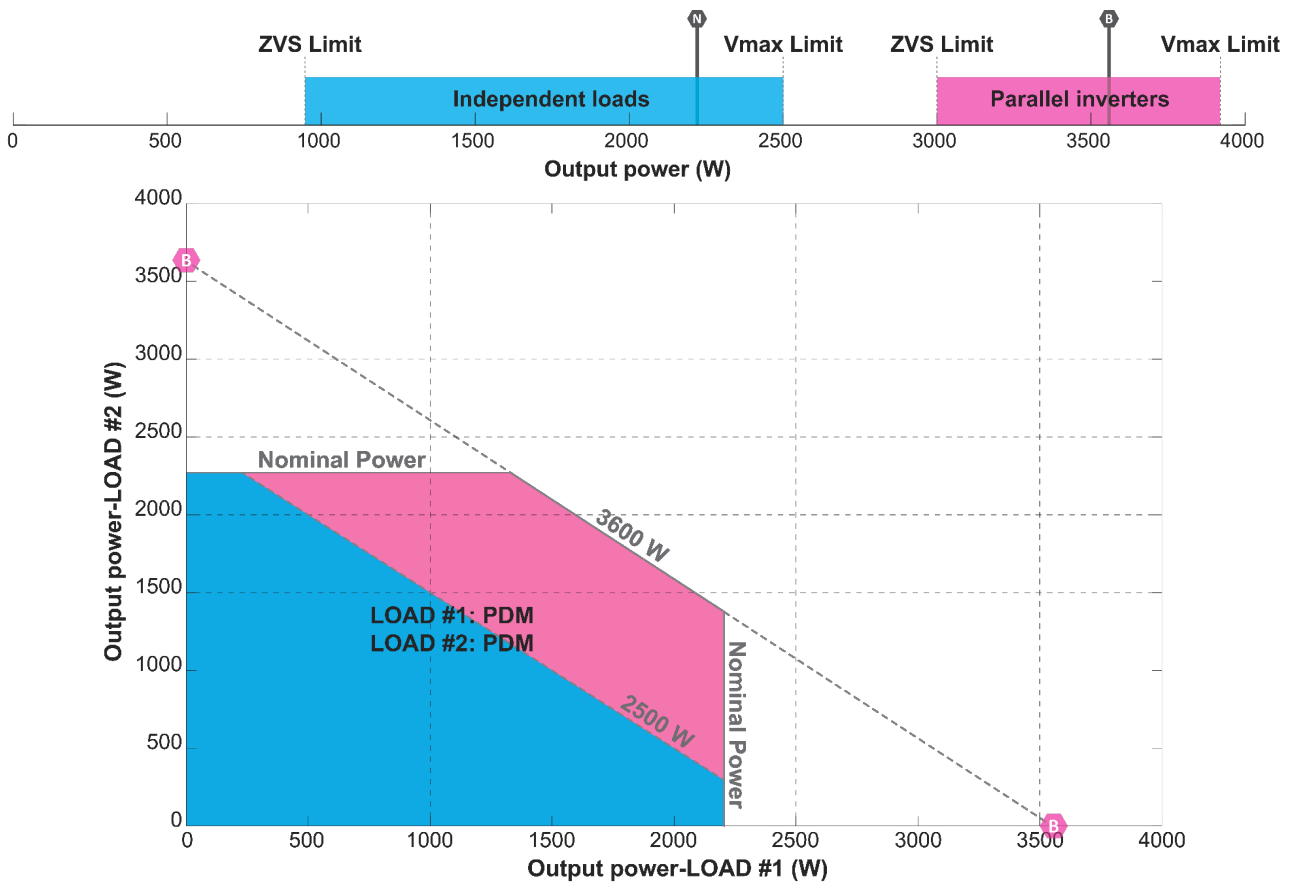

Fig. 9.   Representation of the operating areas for a dual-output induction heating appliance using the proposed power converter topology. The limits established by maximum power and maximum voltage are shown, as well as the control strategies applied in each region.

proposed converter achieves 3.6 kW operation when working with a single load and paralleled capacitor, whereas it also enables 2.2 kW operation with two loads. Moreover, the proposed converter can be optimized to operate in the low-power range avoiding flicker issues typical of this topology. As a conclusion, the proposed converter is able to operate in a wide range of operating conditions using industry standard 1200 V or 1350 V devices, allowing for a high-performance and cost-effective implementation.

B. Proposed control strategy

One of the key challenges when designing a single-switch quasi resonant converter is the design of a control architecture and strategy that ensures soft-switching operation. In the proposed system, the voltage across the switching device is measured, as it shown in Fig. 4, to ensure safe operation while achieving a cost-effective implementation. Besides, the dc-link voltage, V_b, is measured to compute the output power and the switch current I_{sw}, is measured to ensure safe and efficient operation. With this information, it is possible to perform a fast control of the

transistor activation signal to achieve soft-switching at any operating point.

Fig. 8(a) shows a simplified representation of the control algorithm and Fig. 8 (b) shows the main involved waveforms and digital signals. Following this strategy, t_{off} is controlled using the device voltage measurement to achieve soft switching for any given t_{on}, which is selected to deliver the desired output power. The power device on time, t_{on}, is proportional to the output power, and it is controlled to achieve the output power commanded by the user. If the measured output power is lower than the required, t_{on} is increased, and the opposite occurs if the output power needs to be reduced. In order to achieve ZVS, the target is to turn

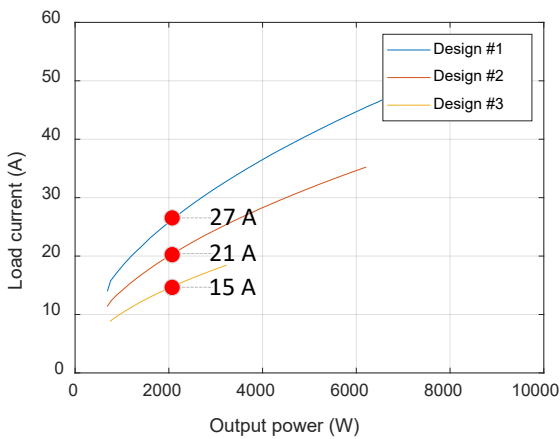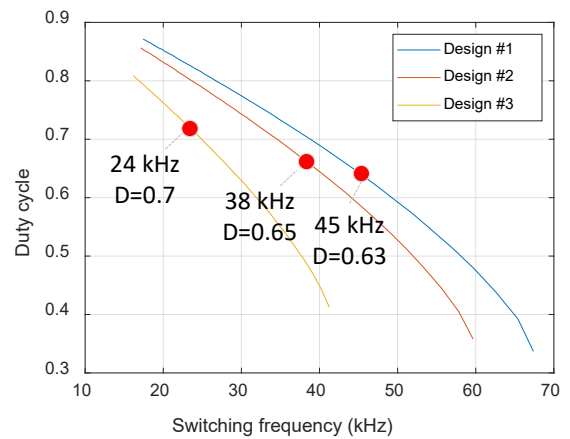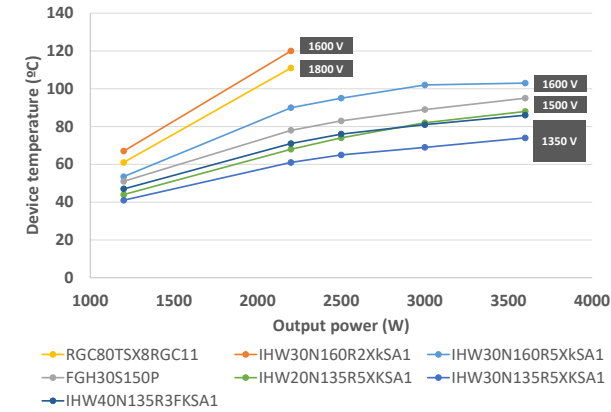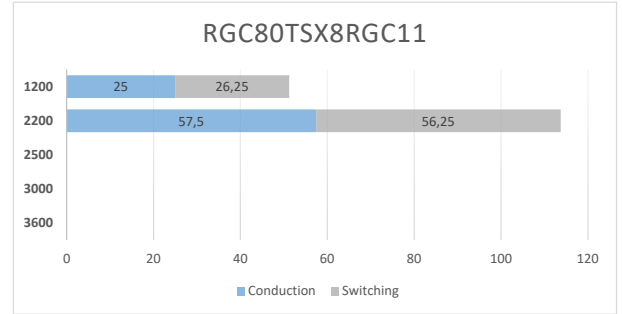|	R_{eq} (Ω)	L_{eq} (µH)	C_r (nF)
Design #1	3	35	120
Design #2	5	50	100
Design #3	9,5	95	90
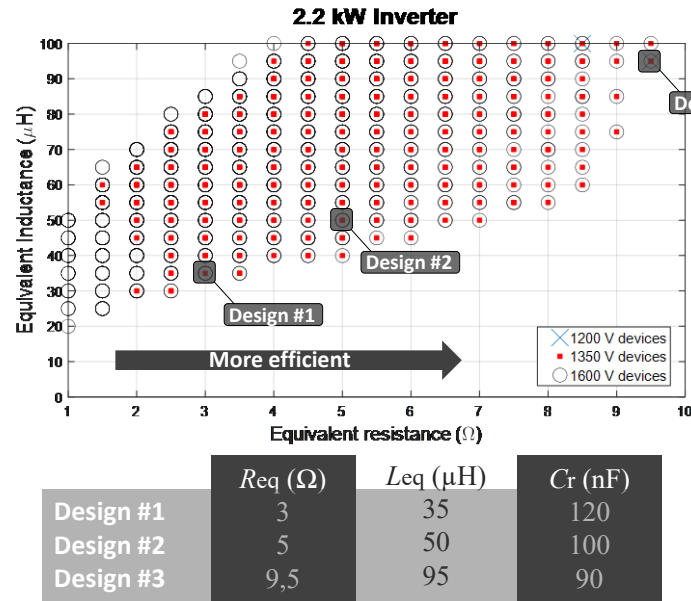
(a)
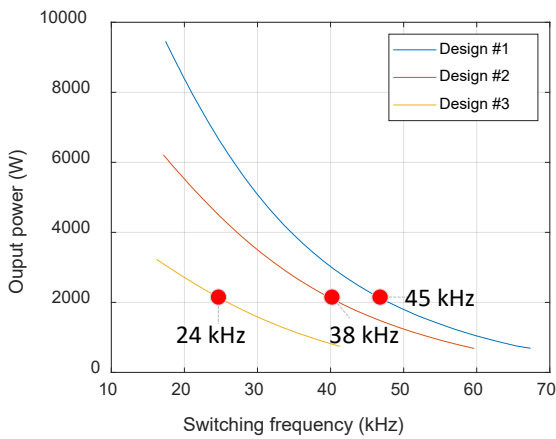
(b)
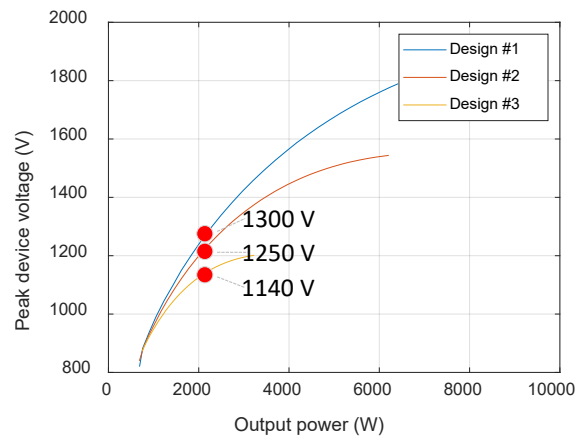
(c)

(d)

(e)

Fig. 10. Design optimization of the experimental prototype considering three alternative designs: Induction coil design window (inductance vs resistance) and required power device voltage (a), output power (b), peak device voltage (c), load current (d) and duty cycle (e).

on the power device when the voltage, V_{sw}, is close to zero. For that, reason, the turn-on transition is triggered when $V_{sw} < V_{th}$, being V_{th} a predefined threshold close to 0. Besides, in order to ensure safe operation, the turn-on transition is also triggered if the voltage across the device exceeds the predefined maximum rating, V_{max}, or if the maximum off time is reached, t_{MAX}. Finally, it is important to remark that this strategy will be implemented using an FPGA-based control architecture as explained in the experimental results section, and it will be implemented using an ASIC design for industrial deployment.
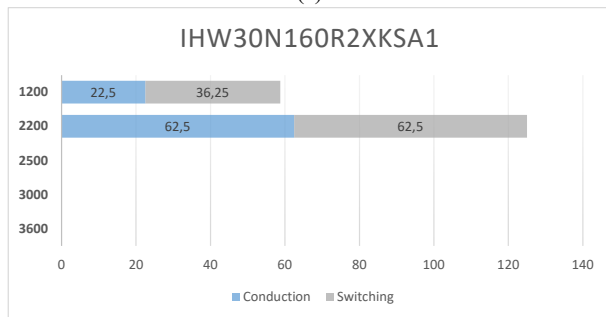
By using the proposed control strategy and reconfigurable topology, it is possible to cover the complete operation range required in a high-performance dual-output induction heating appliance. Fig. 9 shows the operating areas for a dual-output induction heating appliance using the proposed topology and control strategy, and the resonant tank values in Fig. 7, which are the ones used for experimental verification. In this figure, the output power constraints are shown, i.e. maximum total 3600 W, as well as the device maximum voltage ratings. The proposed converter can operate either using independent outputs, up to the individual load nominal power, or paralleled inverters with
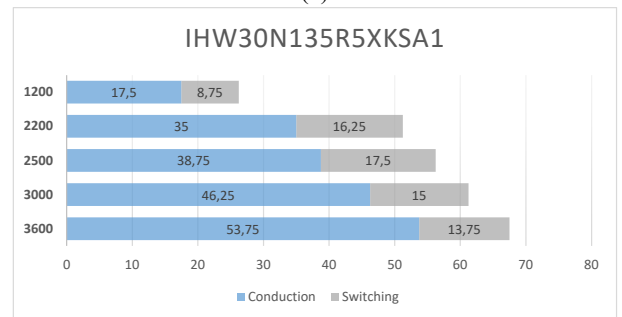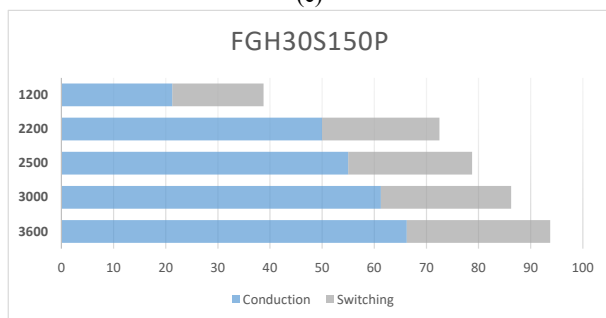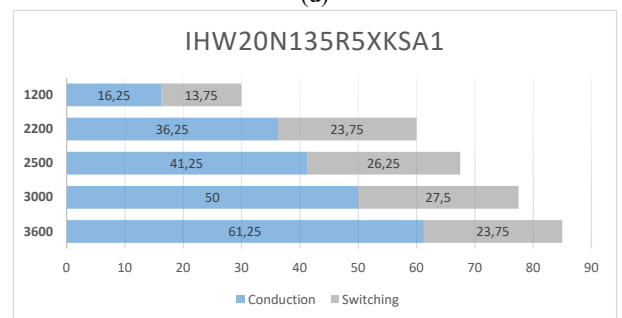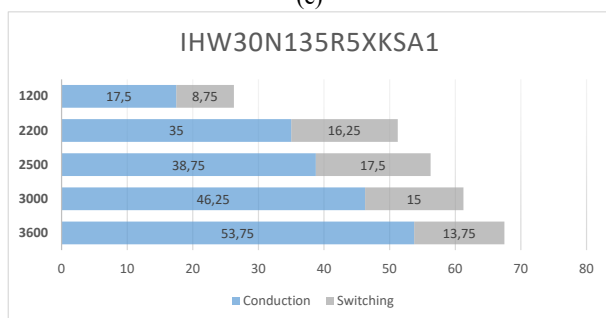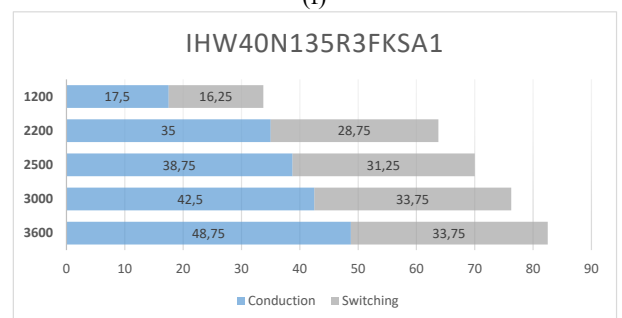

Fig. 11. Power device selection: power device temperature for different output powers (a) and power losses breakdown considering conduction and switching losses for all the analyzed power devices (b-h).

single load to maximize the output power. When required, pulse density modulation (PDM) is applied to achieve the required power combination without compromising ZVS operation or acoustic noise. Besides, the ZVS soft-switching limits in the low output power range are shown. As a conclusion, the proposed topology and control strategy ensure proper output power control in the complete operating conditions map considering a state-of-the-art 3.6 kW induction heating appliance.

III. EXPERIMENTAL PROTOTYPE

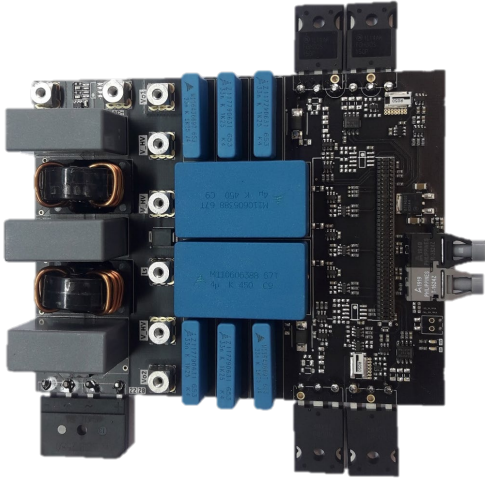In order to test the proposed topology, an FPGA-controlled experimental prototype has been designed and

implemented. It features a dual single-switch quasi-resonant inverter enabling either supplying two IH loads or a single load up to 3.6 kW. To optimize the proposed design, several induction coil designs have been proposed in order to explore the design window, considering the equivalent electrical model and the required voltage in the power devices. Nominal output power, i.e., 2200 W, has been selected as the worst-case design point, since the maximum power point, i.e., 3600 W, will operate with paralleled power devices and reduced voltage due to paralleled resonant capacitors. Fig. 10(a) shows the three proposed designs and the equivalent electrical parameters. This analysis has been completed with the evaluation of the output power (b), peak device voltage (c), load current (d) and duty cycle (e) curves. As a conclusion of this analysis, design #2 has been selected in order to avoid acoustic noise, compared with design #3, and to avoid increased voltage/current values of design #1.

Once the induction coil has been selected, the power devices selection has been analysed. Several IGBT technologies have been considered, ranging from 1350 V up to 1800 V. In order to select the optimum device, a thermal comparison has been performed, and the breakdown of power losses, i.e., conduction and switching losses, has been analysed. Fig. 11(a) shows the power device temperature under different output power conditions. The test was stopped for some devices when the measured temperature was above 120ºC. In this test, the results show that the lower the device blocking voltage the lower the temperature. Fig. 11(b-h) shows a detailed breakdown of the power losses in the devices. This analysis has been performed by placing two series connected devices with only one switching device, allowing to analyse the individual contribution of both

Fig. 12. Dual-output single-switch quasi-resonant experimental prototype.
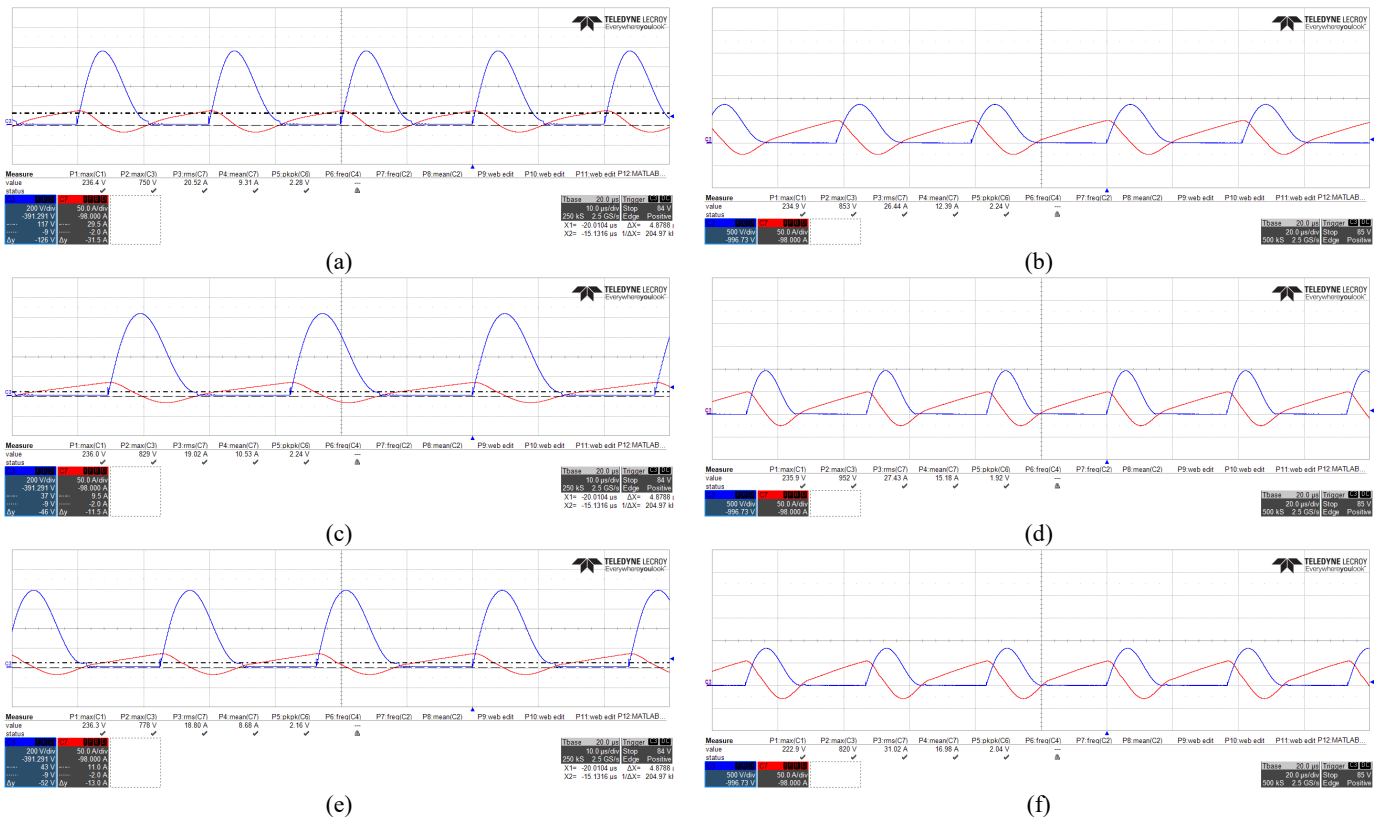

Fig. 13. Main waveforms of the proposed converter operating at nominal output power, i.e. 100 nF and 2200 W (a,c,d), and maximum output power, i.e. 200 nF and 3600 W (b,d,f). Three representative IH loads are used L1 (a,b), L2 (c,d) and L3 (e,f). Main waveforms include device voltage (blue, 200 V/div left and 500 V/div right) and IH coil current (red 500 A/div).
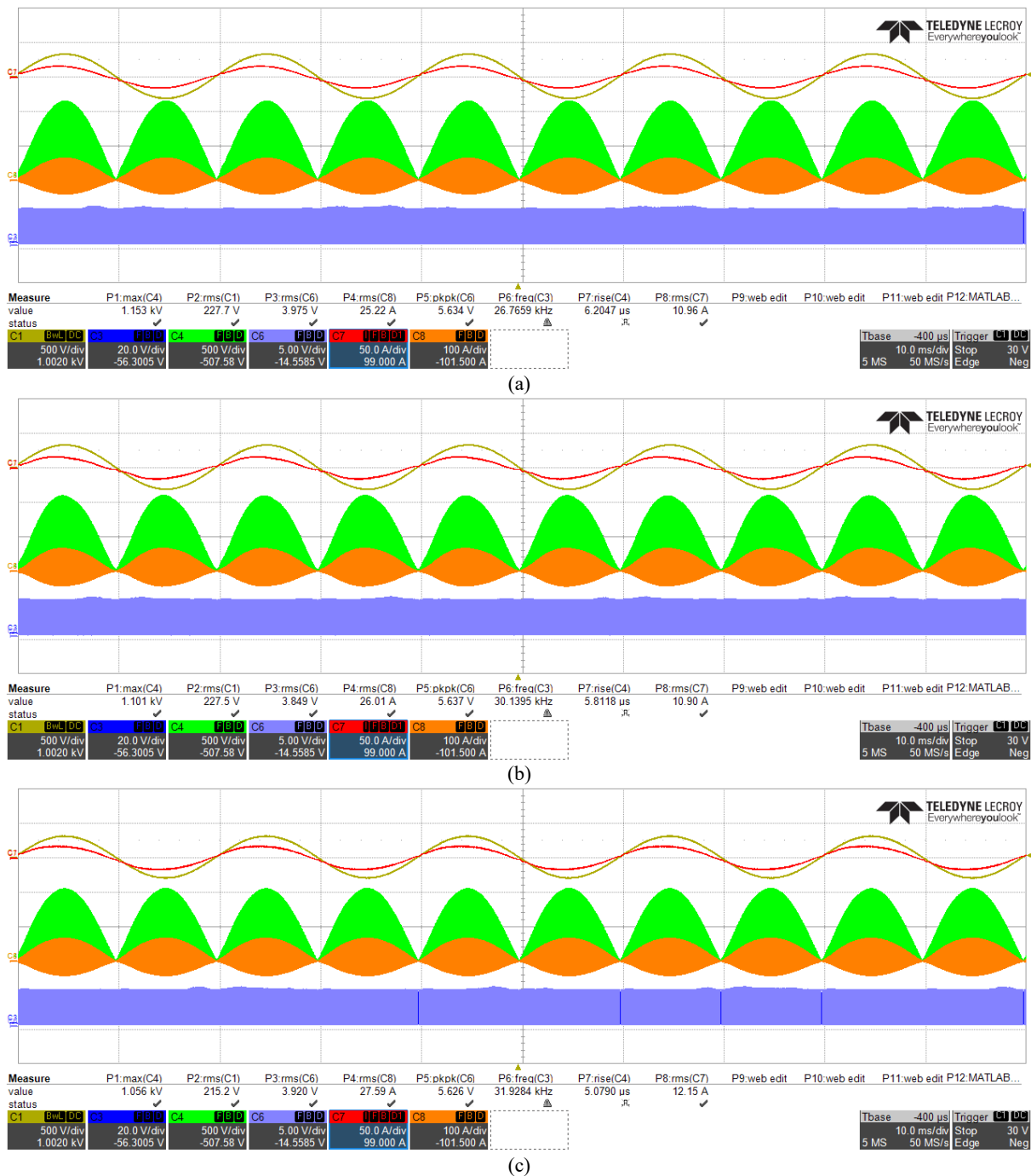
Fig. 14. Main waveforms of the proposed converter with three different representative loads L1 (a), L2 (b), and L3 (c) operating at maximum power, i.e. 3600 W, with 200 nF resonant capacitor. From top to bottom: input voltage (C1, 500 V/div), input current (C7, 50 A/div), device voltage (C4, 500 V/div), IH coil current (C8, 100 A/div), and control signals (C6, 5 V/div).

switching and conduction losses. As a result of these tests, the selected device has been the 1350-V 30-A reverse conducting IGBT IHW30N135R5XKSA1 from Infineon due to both temperature and efficiency considerations. It is important to note that this device performed better due to the appropriate balance between conduction and switching losses, and its thermal performance. Finally, a Xilinx Spartan 6 FPGA is used to implement the proposed modulation and control algorithms. Fig. 12 shows the experimental prototype used in the experiments described below.

Fig. 13 shows the main waveforms of the proposed converter with three different induction heating loads L1 (a,b), L2 (c,d), and L3 (d,f) for both nominal (left side) and maximum output power (right side). Each load has been tested using single resonant capacitor and nominal power, i.e. 100 nF and 2200 W, and maximum power, i.e. 200 nF and 3600 W. These waveforms prove the proper converter operation in the complete output power range for different representative IH loads. In all these cases, soft-switching conditions are met, while the maximum device voltage is not exceeded. These experimental results proves that the proposed topology can operate in an extended operation al range, providing a high-performance and cost-effective implementation.
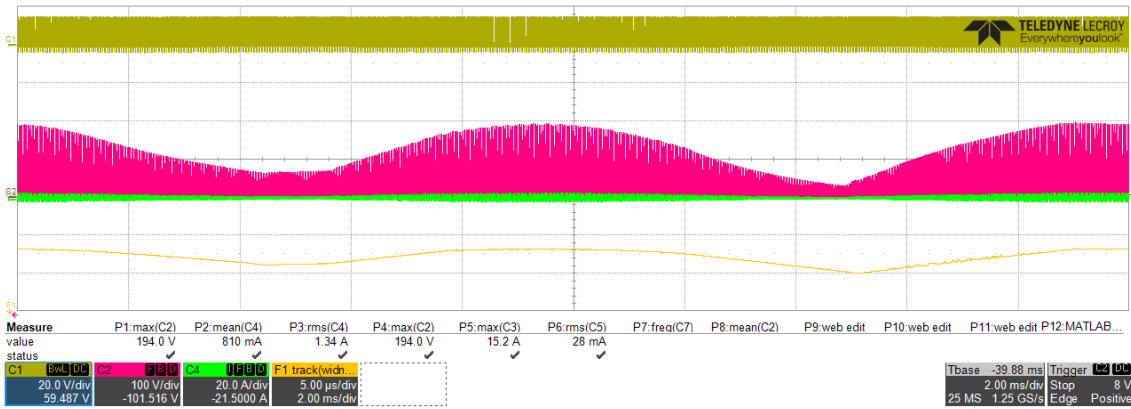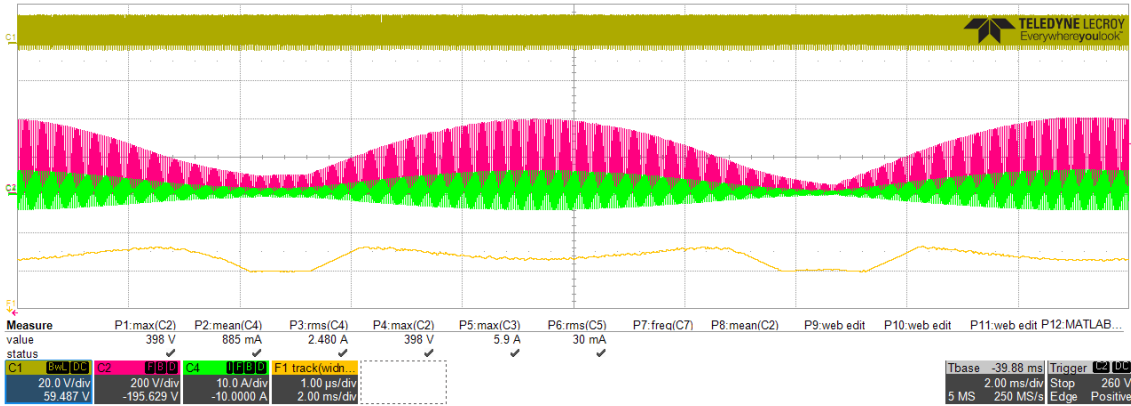
Fig. 15. Main converter waveforms using IH load L1 (a) and L3 (b) with t_{on}=10 μs and controlled t_{off} to achieve soft switching. From top to bottom: control signals (C1, 20 V/div), device voltage (C2, 200 V/div), IH coil current (C4, 20/10 A/div), and math channel representing t_{off} (F1, 1 μs/div).
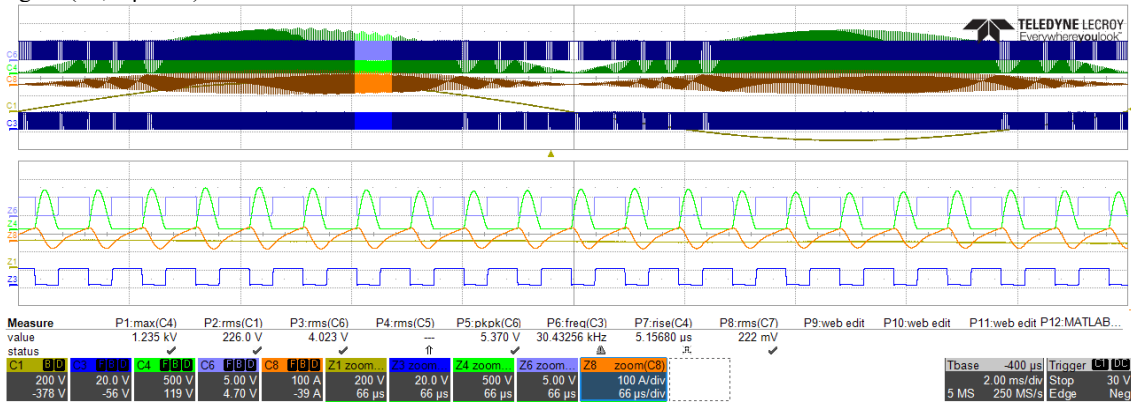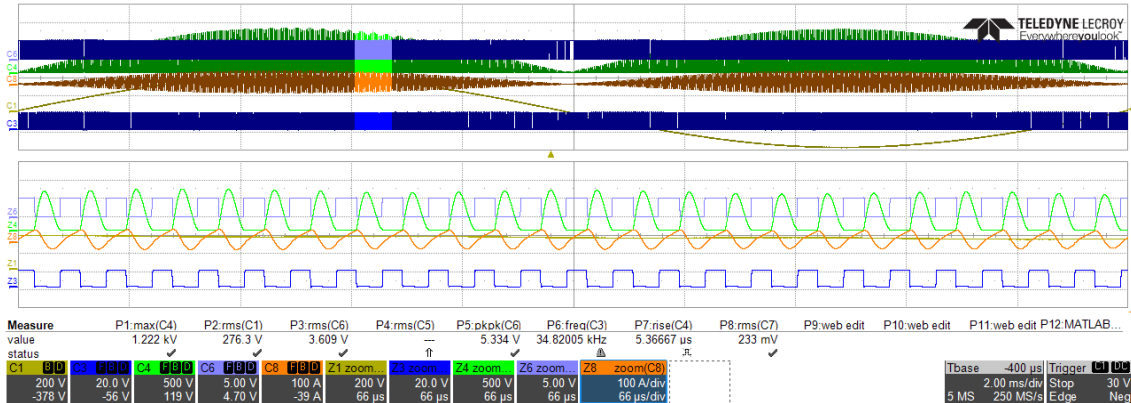
Fig. 16. Experimental waveforms during a mains cycle: The control scheme ensures ZVS during the complete cycle. L1 induction load operating at 230 Vac (a) and 270 Vac (b) with 230 nF resonant capacitor and maximum output power 3600 W. From top to bottom: control signal (C6, 5 V/div), device voltage (C4, 500 V/div), IH coil current (C8, 100 A/div) and mains voltage (C1, 200 V/div).

Fig. 14 shows the converter operation along a mains half-cycle to prove the proper operation of the proposed control algorithm. It has been tested using the same loads L1 (a), L2 (b), and L3 (c) with the maximum power configuration, i.e. 200 nF and 3600 W. In these figures, it can be seen that the proposed converter achieves smooth operation during the mains half-cycle with low current distortion. In order to have a clearer view of the operation of the proposed converter. As a conclusion, the proposed converter is able to operate at full power under real operating conditions. It achieves the same output power performance as state-of-the-art full-resonant half-bridge topologies with a cost-effective implementation.

Fig. 15 represents the operation during a mains half-cycle, where the t_{off} parameter has been represented for a given fixed t_{on}. In this figure, two different IH loads have been used and it can be seen the great dependence of the modulation strategy with the induction heating load. Fig. 15(a) shows a linear material whereas in Fig. 15(b) a non-linear material with strong dependence with the bus voltage is used. This figure shows the proper converter operation and highlights the need of the proposed control strategy to ensure soft-switching in the complete operation range, as the parameter varies significantly during the cycle. This is mainly due to the non-linear behaviour of the induction heating load, which is not easily predictable and depends on the used pot.

Finally, Fig. 16 shows a detail of the converter main waveforms operating at rms ac input voltage of 230 Vac (a) and 270 Vac (b). This test is relevant as it proves the proper converter operation under the maximum voltage for commercial appliances. Besides, the detailed waveforms prove the proper zero voltage switching operation during the mains half-cycle, ensuring efficient soft-switching operation.

IV. CONCLUSIONS

This paper has proposed a high-performance single-switch quasi-resonant inverter for domestic IH applications with extended operation range. The proposed topology takes advantage of a reconfigurable resonant tank to extend the operation range, compared with classical single-switch converters, to increase the maximum output power. Consequently, the proposed topology enables the development of high-performance and cost-effective induction heating. By using the proposed topology, current high-performance state-of-the-art full/half-bridge series resonant topologies can be replaced by a single-switch quasi-resonant inverter with similar performance, achieving a significant cost reduction. The proposed topology has been experimentally tested by using a real scale dual-output inverter, proving the feasibility of the proposed topology. The proposed converter has shown reliable operation, achieving soft-switching and enabling operation up to 3600 W using the proposed topology and control strategy.

REFERENCES

[1] O. Lucía, J. Acero, C. Carretero, and J. M. Burdío, "Induction heating appliances: Towards more flexible cooking surfaces," *IEEE Industrial Electronics Magazine,* vol. 7, no. 3, pp. 35-47, September 2013, doi: 10.1109/MIE.2013.2247795.

[2] O. Lucía, P. Maussion, E. Dede, and J. M. Burdío, "Induction heating technology and its applications: Past developments, current technology, and future challenges," *IEEE Transactions on Industrial Electronics,* vol. 61, no. 5, pp. 2509-2520, May 2014, doi: 10.1109/TIE.2013.2281162.

[3] O. Lucía, H. Sarnago, J. Acero, C. Carretero, and J. M. Burdío, "Induction Heating Cookers: A Path Towards Decarbonization Using Energy Saving Cookers," in *International Power Electronics Conference 2022 IPEC22*, 2022, pp. 1435-1439, doi: 10.23919/IPEC-Himeji2022-ECCE53331.2022.9807062.

[4] W. Feng, F. C. Lee, and P. Mattavelli, "Optimal trajectory control of burst mode for LLC resonant converter," *IEEE Transactions on Power Electronics,* vol. 28, no. 1, pp. 457-466, January 2013, doi: 10.1109/tpel.2012.2200110.

[5] J. M. Leisten, A. K. Lefedjiev, and L. Hobson, "Single ended resonant power supply for induction heating," *Electronics Letters,* vol. 26, no. 12, pp. 814-816, December 1990.

[6] H. Omori, and M. Nakaoka, "New single-ended resonant inverter circuit and system for induction-heating apparatus," *International Journal of Electronics,* vol. 67, no. 2, pp. 277-296, 1989.

[7] H. W. Koertzen, J. A. Ferreira, and J. D. van Wyk, "A comparative study of single switch induction heating converters using novel component effectivity conceps," in *IEEE Power Electronics Specialists Conference*, July 1992, vol. 1, pp. 298-305.

[8] H. Sarnago, O. Lucía, A. Mediano, and J. M. Burdío, "High efficiency parallel quasi-resonant current source inverter featuring SiC MOSFETs for induction heating systems with coupled inductors," *IET Power Electronics,* vol. 6, no. 1, pp. 183-191, 2013, doi: 10.1049/iet-pel.2012.0537.

[9] S. Llorente, F. Monterde, J. M. Burdio, and J. Acero, "A comparative study of resonant inverter topologies used in induction cookers," in *APEC. Seventeenth Annual IEEE Applied Power Electronics Conference and Exposition (Cat. No.02CH37335)*, 10-14 March 2002 2002, vol. 2, pp. 1168-1174 vol.2, doi: 10.1109/APEC.2002.989392.

[10] P. Charoenwiangnuea, S. Wangnipparnto, and S. Tunyasrirut, "Design of A Class-E Direct AC-AC Converter with Only One Capacitor and One Inductor for Domestic Induction Cooker," in *2021 18th International Conference on Electrical Engineering/Electronics, Computer, Telecommunications and Information Technology (ECTI-CON)*, 19-22 May 2021 2021, pp. 679-682, doi: 10.1109/ECTI-CON51831.2021.9454917.

[11] Z. Li, Q. Chen, S. Zhang, X. Ren, and Z. Zhang, "A Novel Domestic SE-IH With High Induction

Efficiency and Compatibility of Nonferromagnetic Vessels," *IEEE Transactions on Industrial Electronics,* vol. 68, no. 9, pp. 8006-8016, 2021, doi: 10.1109/TIE.2020.3013756.

[12] Y. Ishimaru, K. Oka, K. Sasou, K. Matsuse, and M. Tsukahara, "Dual high frequency quasi-resonant inverter circuit by using power MOSFET for induction heating," in *2009 IEEE 6th International Power Electronics and Motion Control Conference*, 17-20 May 2009 2009, pp. 2545-2550, doi: 10.1109/IPEMC.2009.5157833.

[13] S. Wang, K. Izaki, I. Hirota, H. Yamashita, H. Omori, and M. Nakaoka, "Induction-heated cooking appliance using new quasi-resonant ZVS-PWM inverter with power factor correction," *IEEE Transactions on Industry Applications,* vol. 34, no. 4, pp. 705-712, July/August 1998.

[14] S. Okudaira, and K. Matsuse, "Power control of an adjustable frequency quasi-resonant inverter for dual frequency induction heating," in *Proceedings IPEMC 2000. Third International Power Electronics and Motion Control Conference (IEEE Cat. No.00EX435)*, 2000 2000, vol. 2, pp. 968-973 vol.2, doi: 10.1109/IPEMC.2000.884645.

[15] M. Ozturk, F. Zungor, B. Emre, and B. Oz, "Quasi Resonant Inverter Load Recognition Method," *IEEE Access,* vol. 10, pp. 89376-89386, 2022, doi: 10.1109/ACCESS.2022.3201355.

[16] S. Okudaira, and K. Matsuse, "Adjustable Frequency Quasi-Resonant InverterCircuits Having Short-Circuit SwitchAcross Resonant Capacitor," *IEEE Transactions on Power Electronics,* vol. 23, no. 4, pp. 1830-1838, 2008, doi: 10.1109/TPEL.2008.924838.

[17] Y. Kawaguchi, E. Hiraki, T. Tanaka, and M. Nakaoka, "Full bridge phase-shifted soft switching high-frequency inverter with boost PFC function for induction heating system," in *European Conference on Power Electronics and Applications*, 2-5 Sept. 2007 2007, pp. 1-8.

[18] D. Czarkowski, and M. K. Kazimierczuk, "Single-capacitor phase-controlled series resonant converter," *IEEE Transactions on Circuits and Systems,* vol. 40, pp. 383-391, June 1993.

[19] V. Esteve *et al.*, "Improving the efficiency of IGBT series-resonant inverters using pulse density modulation," *IEEE Transactions on Industrial Electronics,* vol. 58, no. 3, pp. 979-987, March 2011.

[20] S. Chudjuarjeen, A. Sangswang, and C. Koompai, "An improved LLC resonant inverter for induction-heating applications with asymmetrical control," *IEEE Transactions on Industrial Electronics,* vol. 58, no. 7, pp. 2915-2925, July 2011.

[21] E. J. Dede, J. V. Gonzalez, J. A. Linares, J. Jordan, D. Ramirez, and P. Rueda, "25-kW/50-kHz generator for induction heating," *IEEE Transactions on Industrial Electronics,* vol. 38, no. 3, pp. 203-209, June 1991, doi: 10.1109/41.87588.

[22] J. M. Espi Huerta, E. J. Dede Garcia Santamaria, R. Garcia Gil, and J. Castello Moreno, "Design of the L-LC resonant inverter for induction heating based on its equivalent SRI," *IEEE Transactions on Industrial Electronics,* vol. 54, no. 6, pp. 3178-3187, December 2007.

[23] A. Fujita, H. Sadakata, I. Hirota, H. Omori, and M. Nakaoka, "Latest developments of high-frequency series load resonant inverter type built-in cooktops for induction heated all metallic appliances," in *IEEE Power Electronics and Motion Control Conference*, 2009, pp. 2537-2544.

[24] H. W. Koertzen, J. D. v. Wyk, and J. A. Ferreira, "Design of the half-bridge series resonant converters for induction cooking," in *IEEE Power Electronics Specialist Conference Records*, 1995, pp. 729-735.

[25] O. Lucía, J. M. Burdío, I. Millán, J. Acero, and L. A. Barragán, "Efficiency oriented design of ZVS half-bridge series resonant inverter with variable frequency duty cycle control," *IEEE Transactions on Power Electronics,* vol. 25, no. 7, pp. 1671-1674, July 2010, doi: 10.1109/TPEL.2010.2042461.

[26] O. Lucía, J. M. Burdío, I. Millán, J. Acero, and D. Puyal, "Load-adaptive control algorithm of half-bridge series resonant inverter for domestic induction heating," *IEEE Transactions on Industrial Electronics,* vol. 56, no. 8, pp. 3106-3116, August 2009, doi: 10.1109/TIE.2009.2022516.

[27] M. Fujun, L. An, X. Xianyong, X. Huagen, W. Chuanping, and W. Wen, "A Simplified Power Conditioner Based on Half-Bridge Converter for High-Speed Railway System," *IEEE Transactions on Industrial Electronics,,* vol. 60, no. 2, pp. 728-738, 2013, doi: 10.1109/tie.2012.2206358.

[28] H. Sarnago, O. Lucía, A. Mediano, and J. M. Burdío, "Multi-MOSFET-based series resonant inverter for improved efficiency and power density induction heating applications," *IEEE Transactions on Power Electronics,* vol. 29, no. 8, pp. 4301-4312, August 2014, doi: 10.1109/TPEL.2013.2288802.

[29] O. Lucía, J. M. Burdío, L. A. Barragán, J. Acero, and I. Millán, "Series-resonant multiinverter for multiple induction heaters," *IEEE Transactions on Power Electronics,* vol. 24, no. 11, pp. 2860-2868, November 2010, doi: 10.1109/TPEL.2010.2051041.

[30] H. Fujita, N. Uchida, and K. Ozaki, "A new zone-control induction heating system using multiple inverter units applicable under mutual magnetic coupling conditions," *IEEE Transactions on Power Electronics,* vol. 26, no. 7, pp. 2009-2017, July 2010.

[31] Y.-C. Jung, "Dual half bridge series resonant inverter for induction heating appliance with two loads," *Electronics Letters,* vol. 35, no. 16, pp. 1345-1346, May 1999.

[32] H. Pham, H. Fujita, K. Ozaki, and N. Uchida, "Phase angle control of high-frequency resonant currents in a multiple inverter system for zone-control induction heating," *IEEE Transactions on Power Electronics,* vol. 26, no. 11, pp. 3357-3366, 2011, doi: 10.1109/TPEL.2011.2146278.

[33] I. Millán, J. M. Burdío, J. Acero, O. Lucía, and D. Palacios, "Resonant inverter topologies for three concentric planar windings applied to domestic induction heating," *Electronics Letters,* vol. 46, no. 17, pp. 1225-1226, Aug 19 2010, doi: 10.1049/el.2010.1197.

[34] H. Sarnago, O. Lucía, A. Mediano, and J. M. Burdío, "Class-D/DE dual-mode-operation resonant converter for improved-efficiency domestic induction heating system," *IEEE Transactions on Power Electronics,* vol. 28, no. 3, pp. 1274-1285, Mar 2013, doi: 10.1109/TPEL.2012.2206405.

[35] J. I. Rodriguez, and S. B. Leeb, "A multilevel inverter topology for inductively coupled power transfer," *IEEE Transactions on Power Electronics,* vol. 21, no. 6, pp. 1607-1617, 2006.

[36] J. I. Rodriguez, and S. B. Leeb, "Nonresonant and resonant frequency-selectable induction-heating targets," *IEEE Transactions on Industrial Electronics,* vol. 57, no. 9, pp. 3095-3108, September 2010. [Online]. Available: 10.1109/TIE.2009.2037676.

[37] H. Sarnago, A. Mediano, and O. Lucía, "High efficiency ac-ac power electronic converter applied to domestic induction heating," *IEEE Transactions on Power Electronics,* vol. 27, no. 8, pp. 3676-3684, August 2012, doi: 10.1109/TPEL.2012.2185067.

[38] O. Lucía, F. Almazán, J. Acero, J. M. Burdío, and C. Carretero, "Multiple-output resonant matrix converter for multiple-inductive-load systems," in *IEEE Applied Power Electronics Conference and Exposition*, 2011, vol. 1, pp. 1338-1343.

[39] H. Sugimura, S.-P. Mun, S.-K. Kwon, T. Mishima, and M. Nakaoka, "High-frequency resonant matrix converter using one-chip reverse blocking igbt-based bidirectional switches for induction heating," in *IEEE Power Electronics Specialists Conference*, June 2008.

[40] N. Nguyen-Quang, D. A. Stone, C. Bingham, and M. P. Foster, "Comparison of single-phase matrix converter and H-bridge converter for radio frequency induction heating," in *European Conference on Power Electronics and Applications*, 2007, pp. 1-9.

[41] H. Sarnago, O. Lucía, and J. M. Burdío, "High-Performance Class-E Quasi-Resonant Inverter for Domestic Induction Heating Applications," in *IEEE Applied Power Electronics Conference and Exposition*, 2022, pp. 1202-1207.

[42] C. Carretero, O. Lucía, J. Acero, R. Alonso, and J. M. Burdío, "Frequency-dependent modeling of domestic induction heating systems using numerical methods for accurate time-domain simulation," *IET Power Electronics,* vol. 5, no. 8, pp. 1291-1297, September 2012, doi: 10.1049/iet-pel.2012.113.

[43] H. Sarnago, O. Lucía, and J. M. Burdio, "A Versatile Resonant Tank Identification Methodology for Induction Heating Systems," *IEEE Transactions on Power Electronics,* vol. 33, no. 3, pp. 1897-1901, Mar 2018, doi: 10.1109/TPEL.2017.2740998.

[44] O. Jiménez, O. Lucía, I. Urriza, L. A. Barragán, and D. Navarro, "Analysis and implementation of FPGA-based online parametric identification algorithms for resonant power converters," *IEEE Transactions on Industrial Informatics,* vol. 10, no. 2, pp. 1144-1153, May 2014, doi: 10.1109/TII.2013.2294136

[45] A. L. Shenkman, "Transient Analysis of Electric Power Circuits Handbook," *Springer,* The Netherlands, 2005.